

Heterogeneous & Homogeneous & Bio- & Nano-

CHEMCATCHEM

CATALYSIS

Accepted Article

Title: Highly active noble metal-free copper-hydroxyapatite catalysts for toluene total oxidation

Authors: Dayan Chlala, Jean-Marc Giraudon, Nicolas Nuns, Madona Labaki, and Jean-François Lamonier

This manuscript has been accepted after peer review and appears as an Accepted Article online prior to editing, proofing, and formal publication of the final Version of Record (VoR). This work is currently citable by using the Digital Object Identifier (DOI) given below. The VoR will be published online in Early View as soon as possible and may be different to this Accepted Article as a result of editing. Readers should obtain the VoR from the journal website shown below when it is published to ensure accuracy of information. The authors are responsible for the content of this Accepted Article.

To be cited as: *ChemCatChem* 10.1002/cctc.201601714

Link to VoR: <http://dx.doi.org/10.1002/cctc.201601714>

Highly active noble metal-free copper-hydroxyapatite catalysts for toluene total oxidation

Dayan Chlala,^[a,b] Jean-Marc Giraudon,^[a] Nicolas Nuns,^[a] Madona Labaki,^[b] and Jean-François Lamonier*^[a]

Abstract: Hydroxyapatite (Hap) - supported copper materials prepared by the wet impregnation method were designed as noble metal-free catalysts for toluene total oxidation. Cu/Hap with different Cu loading (from 2.5 wt% to 20 wt%), calcined at 400 °C, were characterized by inductively coupled plasma optical emission spectroscopy, N₂ physisorption, X-ray diffraction, Raman, infrared, X-ray photoelectron and time-of-flight secondary ion mass spectroscopies. Tenorite CuO phase was detected in all materials, while additional libethenite Cu₂(PO₄)OH phase was observed for sample with 20 wt% Cu. The presence of libethenite was accompanied by the formation of Ca₂CO₃H⁺ ions at the hydroxyapatite surface. Residual NO₃⁻ species in interaction with Cu and Ca were also found, their amount increasing with Cu content in the sample. Interestingly the specific activity in the toluene total oxidation increased with the decrease in Cu content in the catalyst. The rate per mole of copper was increased 10 times when the copper content was 4 times reduced. This noticeable result could be related to the presence of acid sites with moderate strength as well as fine dispersed CuO species on the hydroxyapatite, allowing the toluene molecules activation and their oxidation through a redox mechanism. Moreover Cu_{2.5}wt%/Hap showed remarkable stable catalytic performance for 45 h time-on-stream, providing evidence that this material has a high potential for Volatile Organic Compound catalytic removal application.

Introduction

Volatile Organic Compounds (VOC) are an important group of air pollutants which particularly harm human health and environment. Among them toluene is widely distributed in the environment. The main source of release into the environment is related to the high presence of toluene in gasoline. In this case, toluene is emitted either directly during the vaporization of gasolines (petrol station, transport and storage of fuels ...), or in the exhaust gases of gasoline-powered vehicles (unburned, volatilization, etc.). Other emissions come from the vapors of toluene used as a solvent, production discharges and incineration discharges.

One of the best efficient methods to reduce this harmful VOC in environment is the catalytic total oxidation in air into carbon dioxide and water.^[1] This technology saves energy by shifting to lower values the temperature needed for non-catalytic oxidation, as well as it reduces the noxious byproducts formation.^[2,3] Although supported noble metal based catalysts show excellent activities for the VOC total oxidation at low temperatures,^[4,5] their high cost limit their wide applications. Thus, the design and development of economic noble metal-free catalysts with comparable or superior activity and stability than noble metal or noble metal oxide based catalysts is a major research area for the sake of development of more sustainable industrial chemical processes.

Transition metal oxides have been found to be active in VOC oxidation. Moreover in comparison with noble metals these oxides show lower cost, superior resistance to poisoning and higher thermal stability.^[6,7] However their activity at low temperature must be improved in order to compete noble metal based catalysts.

Copper oxides are considered to be active and selective in the oxidation of toluene.^[8,9] Wang^[10] demonstrated that copper deposited on alumina exhibited the best catalytic performance with respect to the complete oxidation of toluene among the different transition metals (Fe, Mn, Cr, Co, Mo and Ni). In addition, Saqer *et al.*^[11] found that copper oxide supported on γ -Al₂O₃ exhibits the highest catalytic activity in the oxidation of toluene (about 100 % conversion at 350 °C) compared to the other transition metal oxides (CeO₂, CsO, ZrO₂, MnO, V₂O₅, MgO, Nd₂O₃ and Cr₂O₃). This result was linked to the better dispersion of the active phase on this support.

Another key parameter that controls the activity, selectivity and stability of the supported metal oxides materials is the support composition. Deng *et al.*^[12] found that by incorporation of appropriate amount of ZrO₂ in Cu-CeO₂ systems, the oxygen mobility of the support is enhanced and the toluene oxidation is achieved at lower temperature. Carabineiro *et al.*^[13] correlated the total acidity of the catalysts and their activity in toluene oxidation, highlighting the role of acidity in the VOC oxidation process. High concentration of acid sites with moderate strength was favorable for the catalytic activity.

Hydroxyapatite Ca₁₀(PO₄)₆(OH)₂ (Hap) based materials, are safe, non-toxic and inexpensive, and have attracted great attention in several fields such as medical and biological applications, applications in archeology, optics and in chemical applications.^[14] Furthermore, these compounds present a high chemical and thermal stability, and have a structural flexibility. First, Hap contains both acidic and basic sites with moderate strength^[15] in a single crystal lattice, hence it can be used in reactions requiring bifunctional solid catalyst, such as the Friedel-Crafts reactions^[16] and the Guerbet reaction.^[17] Chen *et al.*^[18] have prepared Manganese oxides loaded on various supports (SBA-15, MgO,

[a] D. Chlala, J.-M. Giraudon, N. Nuns, J.-F. Lamonier
Univ. Lille, CNRS, Centrale Lille, ENSCL, Univ. Artois, UMR 8181 – UCCS – Unité de Catalyse et Chimie du Solide, F-59000 Lille, France
E-mail: jean-francois.lamonier@univ-lille1.fr

[b] D. Chlala, M. Labaki
Lebanese University, Laboratory of Physical Chemistry of Materials (LCPM)/PR2N, Faculty of Sciences, Fanar, BP 90656, Jdeidet El Metn, Lebanon

Supporting information for this article is given via a link at the end of the document.

FULL PAPER

Al₂O₃, TiO₂ and Hap) with different acid-base properties, to study the direct imine formation by oxidative coupling of alcohols and amines. They reported that hydroxyapatite (with amphoteric nature) supported manganese oxides (MnOx/Hap) showed the best activity and selectivity for this reaction compared to the inert (SBA-15), basic (MgO) or acidic (Al₂O₃ and TiO₂) support. Furthermore Hap is recognized for its ability to easily exchange calcium ions exposed on the surface. For example the doping of Hap with a Cu active phase has been achieved by Qu *et al.*^[19] Five possible sites for Cu location has been proposed based on the Hap structure and experimental results. Qu *et al.* claimed that owing to the method of preparation (impregnation or co-precipitation) copper location can be adjusted in the Hap structure. Recently, hydroxyapatite was used for the first time as a support for Pd and Mn species in the VOC catalytic oxidation removal.^[20,21] The Pd based catalytic formulations competed with the best palladium systems described in literature, showing an evidence that hydroxyapatite support could substitute conventional ones such as zeolite or alumina. Indeed at 150 °C, the specific rates on hydroxyapatite supports were found to be four to six times higher than the specific rate on alumina support in the toluene oxidation reaction.^[20] As for manganese,^[21] we found that the hydroxyapatite support allowed to get well dispersed MnOx species using Mn(II) nitrate as Mn source and total conversion of toluene at 220 °C was obtained over MnNit-Hap catalyst. Finally Aellach *et al.*^[22] demonstrated the effect of the Co species introduction in the Hap material on their catalytic performances in the methanol total oxidation. Better Co₃O₄ species reducibility and activity were obtained when Co species have been wet impregnated on hydroxyapatite. The goal of the present study was to investigate how the amount of impregnated Cu influences the performance of Cu/hydroxyapatite when operating in the reaction of toluene oxidation. In particular the effect of copper loading was evaluated on the activity, selectivity and stability of Cu/Hap materials and discussed in relation to their physicochemical properties.

Results and Discussion

1. Catalyst characterizations

1.1. Structural and textural characterizations

The chemical composition values (**Table 1**) indicate that for the impregnated samples, copper content was close to that expected. The X-ray diffraction patterns obtained at room temperature for Hap and CuxHap materials calcined at 400 °C are shown in **Figure 1**. The Hap solid exhibits diffraction lines corresponding to the hydroxyapatite phase Ca₅(PO₄)₃OH (PDF no. 00-009-0432) confirming that the hydroxyapatite crystallizes in the hexagonal system with space group P6₃/m.

The impregnation of copper on Hap does not affect the structure of the support as its diffraction peaks position and intensity do not significantly change with the addition of Cu and no loss of crystallinity is observed.

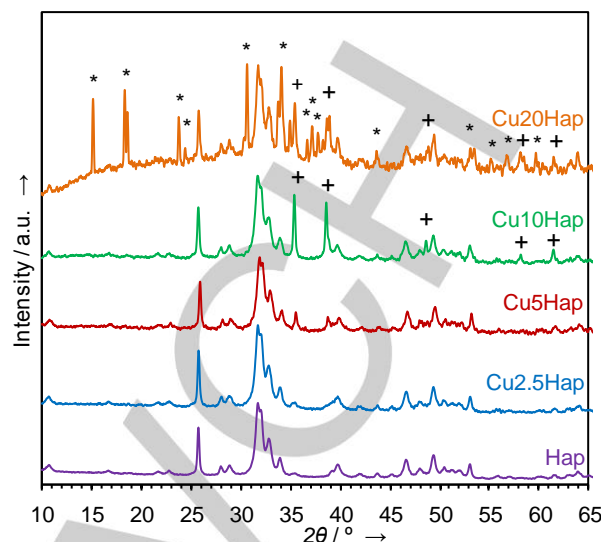


Figure 1. XRD patterns of pure Hap and CuxHap samples
+ : CuO (PDF no. 00-048-1548) and * : Cu₂(PO₄)(OH) (PDF no. 01-077-0922)

The CuO monoclinic phase (PDF no. 00-048-1548) known as tenorite with space group C2/c (five diffraction peaks marked by (+) in **Figure 1**) has been detected in all the CuxHap samples. The intensity of these peaks increased with the copper content from 2.5 to 10 wt%, and then remained constant for the content of 20 wt% of copper. An additional phase (fourteen diffraction peaks marked with (*) in **Figure 1**) corresponding to the orthorhombic phase Cu₂(PO₄)(OH) (PDF no. 01-077-0922) known as libethenite with space group Pnmm is clearly observed for Cu₂₀Hap sample. The mean crystallite size of CuO and Cu₂(PO₄)(OH) determined from the Rietveld refinement are summarized in **Table 1**. The crystallite size of CuO increased from 12 to 42 nm with copper increase up to 10 wt% and then slightly decreased to 33 nm for Cu₂₀Hap sample. For the latter, the Cu₂(PO₄)(OH) crystallite size is 78 nm.

Table 1. Chemical composition, crystallite size and textural properties of the samples

Sample	Cu wt. %	D _c ^[a] CuO / nm	D _c ^[a] Cu ₂ PO ₄ OH / nm	SSA / m ² .g ⁻¹	V _p ^[c] / cm ³ .g ⁻¹	D _p ^[d] / nm
Hap	-	-	-	103	0.58	57
Cu _{2.5} Hap	2.8	12	-	92(92) ^[b]	0.47	50
Cu ₅ Hap	5.2	36	-	85	0.45	50
Cu ₁₀ Hap	9.8	42	-	72(95) ^[b]	0.35	55
Cu ₂₀ Hap	16.7	33	78	21	0.12	63

[a] Crystallite size. [b] After test of stability. [c] Pore volume. [d] BJH desorption maximum pore diameter

FULL PAPER

The nitrogen adsorption-desorption isotherms for Hap and Hap-supported Cu samples (**Figure S1**) display the characteristic hysteresis loop of a Type IV isotherm (IUPAC) lying in the P/P° range of 0.7-1 exhibiting mesoporous character. However the pore diameter of all the solids (not shown here) is non-uniform and exhibited a broad distribution ranging from 5 to 160 nm, with the maximum distribution of pore at around 57 ± 7 nm.

The specific surface area (SSA) and pore volume values of Hap were $103 \text{ m}^2\cdot\text{g}^{-1}$ and $0.58 \text{ cm}^3\cdot\text{g}^{-1}$, respectively. These values decrease when Cu content increases in the sample. For Cu20Hap the decrease is much more pronounced, the SSA and pore volume values being reduced by a factor of about 5 (**Table 1**). This can be explained by a partial blocking of the pores of the support by CuO and $\text{Cu}_2(\text{PO}_4)(\text{OH})$ crystallites, both phases identified by XRD in Cu20Hap.

1.2. Infrared and Raman analyses

Figure 2 shows the IR spectra of Hap and Cu_xHap materials focused on $500\text{-}4000 \text{ cm}^{-1}$ region. No shift in wavenumber was observed for the different vibration bands.

The PO_4 vibrational modes are observed at 565 cm^{-1} , 602 cm^{-1} , 962 cm^{-1} and $1030\text{-}1100 \text{ cm}^{-1}$, as reported previously.^[23,24] The presence of adsorbed water is also detected in the range $3300\text{-}3600 \text{ cm}^{-1}$ and at about 1637 cm^{-1} . The stretching and bending vibration modes of OH structural groups are detected at 3572 and 633 cm^{-1} , respectively. The presence of CO_3^{2-} species with characteristic vibration bands located at 872 cm^{-1} , 1450 cm^{-1} and 1419 cm^{-1} is confirmed in all the materials.^[25,26] Furthermore, HPO_4^{2-} groups might also be present, with the characteristic vibration band at 872 cm^{-1} . However, this latter overlaps with the carbonate vibration band, making straightforward conclusions impossible.^[27] In addition, the presence of residual NO_3^- species is attested by the presence of a sharp nitrate band in the vicinity of 1385 cm^{-1} . Copper addition to the hydroxyapatite support results in an increase in the intensity of this absorption band. This result indicates an incomplete nitrate decomposition even after the calcination step (4 h at $400 \text{ }^\circ\text{C}$ in air flow). For Cu20Hap sample the NO_3^- band is very intense. This is also accompanied by an increase in the intensity of the absorption band characteristic of carbonates. Moreover, the infrared spectrum of Cu20Hap shows additional bands (represented by * in **Figure 2**) corresponding to (i) the stretching and bending vibrations of OH units in the libethenite phase detected at 3405 cm^{-1} (with a shoulder at 3457 cm^{-1}) and 810 cm^{-1} , respectively and (ii) the PO_4 groups observed at 646 cm^{-1} , 917 cm^{-1} and 969 cm^{-1} .^[28] This result is in agreement with XRD one.

Figure 3 shows the Raman scattering spectra of the various materials. Hap sample exhibits the characteristic peaks of the hydroxyapatite phase, since the line positions of the phosphate vibration modes given in **Table 2** are in agreement with those of the literature.^[22]

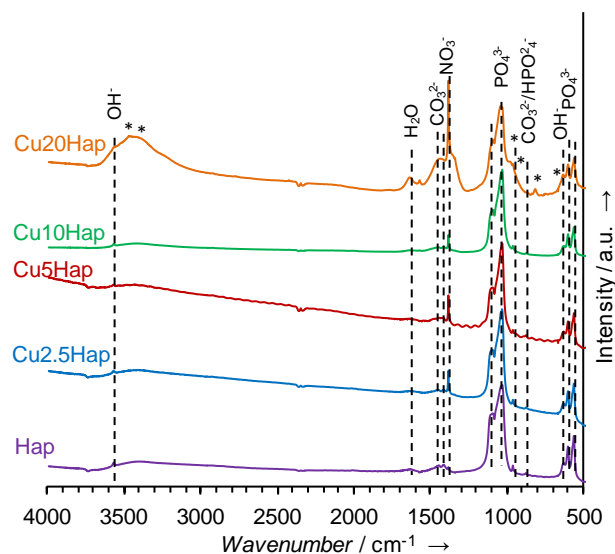


Figure 2. FT-IR spectra of Hap and Hap-supported Cu materials focused on $500\text{-}4000 \text{ cm}^{-1}$

For the copper impregnated solids, additional peaks at 294 cm^{-1} , 343 cm^{-1} and 627 cm^{-1} are observed (**Figure 3a**). These lines are attributed to CuO ^[29] and their intensities are increasing with the copper content in the solid.

Table 2. Raman line positions and assignment for the investigated materials

Sample	Wavenumber / cm^{-1}				
	Hap (H)	CuO (C)	$\text{Cu}_2\text{PO}_4\text{OH}$ (L)	CO_3^{2-} (G)	NO_3^- (N)
Hap	429,446,578, 588,606,962, 1047,1076	-	-	-	-
Cu2.5Hap	428,445,578, 588,606,962, 1042,1076	294,342, 627	-	-	-
Cu5Hap	428,444,578, 587,605,961, 1041,1076	295,341, 627	-	-	-
Cu10Hap	427,445,578, 586,609,961, 1048,1076	293,341, 627	-	-	-
Cu20Hap (1)	430,452,579, 593,606,960	299,345, 629	-	740	1056
Cu20Hap (2)	450,960	299,347, 627	299,453, 554,621, 648,980, 1020	738	1056
Cu20Hap (3)	450,579,960	299,348, 632	-	738, 1066	-

FULL PAPER

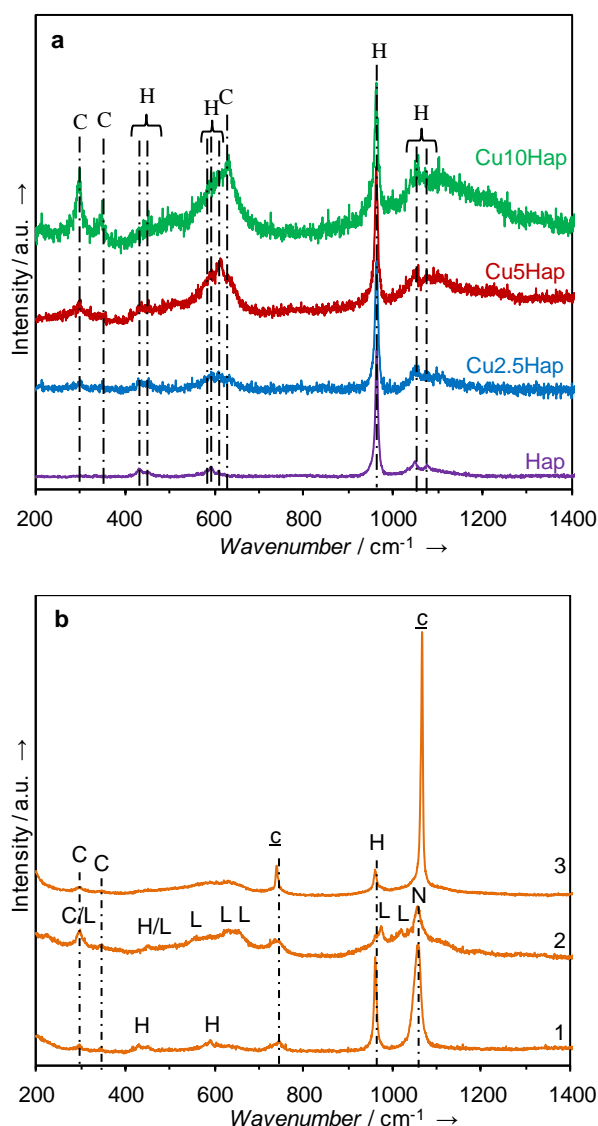


Figure 3. Raman spectra of (a) Hap, Cu2.5Hap, Cu5Hap and Cu10Hap and (b) Cu20Hap. (H: Hap; C: CuO; L: Cu₂(PO₄)(OH); N: NO₃⁻ and G: CO₃²⁻)

Laser beam focused on different locations led to different Raman spectra for Cu20Hap, suggesting an heterogeneity in the composition of this sample (Figure 3b). New lines have been detected in addition to the characteristic lines of the Hap and CuO phases. Spectrum 1 shows an intense peak at 1056 cm⁻¹ characteristic of nitrates^[30,31] and another peak at about 740 cm⁻¹ which could be attributed to carbonates inserted in hydroxyapatite.^[32] Spectrum 2 reveals seven other lines at 299, 453, 554, 621, 648, 980 and 1020 cm⁻¹ likely related to the libethenite phase.^[33] In spectrum 3 two lines are clearly observed at 738 and 1066 cm⁻¹ which can be derived from two characteristic vibrational modes of the CO₃²⁻ group inserted in hydroxyapatite.^[32,34,35]

Thus, these three Raman spectra indicate the presence of two different copper phases for the Cu20Hap solid: CuO and Cu₂(PO₄)(OH) in addition to the presence of residual NO₃⁻ and CO₃²⁻, whether or not included in hydroxyapatite. Finally, the Raman results are in agreement with the IR results which showed the presence of the nitrate and carbonate bands in higher intensity for this sample compared to the other solids.

1.3. XPS analyses

For Hap and CuxHap samples, the binding energy (BE) values for Ca 2p_{3/2}, P 2p_{3/2} and O 1s were found to be at 347.7, 133.5 and 531.6 eV (± 0.3 eV), respectively. These BE values are similar to those reported for pure hydroxyapatite in the literature,^[36,37] suggesting that copper species do not influence significantly the chemical environment of these species.

The XPS spectra of the N 1s region (Figure S2) show typically 3 photopeaks located at 400, 404 and 408 eV. The low BE photopeak belongs likely to ammonium groups and could be related to the use of (NH₄)₂PO₄ precursor for the synthesis of the hydroxyapatite support. The two other photopeaks at 404 and 408 eV have been assigned respectively to nitrite and nitrate ions originating most probably from the Cu(NO₃)₂·3H₂O precursor. The contribution of nitrates to N 1s region increases with the copper content in agreement with the IR results.

Due to the *in-situ* copper species reduction during the XPS analysis it has not been possible to study the copper oxidation state in CuxHap. It is interesting to notice that the greater the copper content in the sample is, the less this *in-situ* reduction phenomenon will be visible in the Cu 2p spectrum. For Cu20Hap sample, copper species are retained as Cu²⁺ along the XPS analysis, while for CuxHap (2.5 wt.% ≤ x ≤ 10 wt.%) reduced copper (Cu⁺ and/or Cu⁰) was detected on the surface. Semi-quantitative XPS analysis is however possible. Bulk and XPS Cu/(Ca+P) ratios are listed in Table 3. In a general way, XPS Cu/(Ca+P) ratios are lower than those obtained from ICP analysis except in the case of Cu2.5Hap for which the two ratios are almost equal. When copper content in the material increases, the difference between the two ratios increases (Table 3). That means, when the copper loading increases, part of the copper becomes not visible by XPS, and consequently can be suspected to be present in the form of >10 nm particles (taking into account that the analysis depth of XPS is close to this value).

Table 3. Atomic bulk and surface ratios for CuxHap samples; T₁₀, T₅₀, T₉₀ and obtained in toluene oxidation for Hap and CuxHap catalysts

Solid	Cu/(Ca+P) ICP	Cu/(Ca+P) XPS	T ₁₀ / °C	T ₅₀ / °C	T ₉₀ / °C	E _A , kJ.mol ⁻¹
Hap	-	-	293	390	>400	-
Cu2.5Hap	0.030	0.027	196	215	231	108
Cu5Hap	0.057	0.024	200	220	238	114
Cu10Hap	0.122	0.038	208	232	246	124

FULL PAPER

Cu20Hap	0.267	0.091	223	248	277	158
---------	-------	-------	-----	-----	-----	-----

This result is in line with the evolution of mean crystal domain size evaluated from X-ray line broadening of XRD patterns. With average crystallite size of 12 nm for CuO in Cu2.5Hap sample (**Table 1**), whole copper is expected to be visible by XPS. Besides XPS and bulk Cu/(Ca+P) ratio values are very close. With mean crystal domain sizes for CuO higher than 33 nm in CuxHap ($x \geq 5$ wt.%) samples (**Table 1**), copper is not expected to be fully observable by XPS, that explains why XPS Cu/(Ca+P) ratio becomes significantly lower than those obtained from ICP analysis (**Table 3**).

1.4. ToF-SIMS analyses

ToF-SIMS has been performed in order to get understandings into the elemental composition in the outer-most atomic layers of samples. The high sensitivity of the ToF-SIMS analysis (study of trace levels up to 1 ppm) allows to provide molecular information about surface and interfaces of the materials through the detection of molecular ions.

It is found the characteristic secondary ions of hydroxyapatite in the negative and positive spectra of Hap (**Figure S3**), as previously reported.^[21] The ToF-SIMS spectra of the CuxHap samples identify the presence of residual NO_3^- in interaction with copper and calcium demonstrated by the presence of the CaNO_2^+ and CuNO_3^- ions with $m/z = 86$ and 125.5 respectively. **Figure 4** clearly shows that the intensity of these ions increases when copper is added to Hap. This increase is moderate and in the same extent for Cu2.5Hap, Cu5Hap and Cu10Hap. However for Cu20Hap a huge increase of CaNO_2^+ and CuNO_3^- normalized intensities is observed, which is in agreement with IR results.

Moreover, Cu_2PO_4^- ion ($m/z = 222.8$) was detected only in the ToF-SIMS (-) spectrum of Cu20Hap solid, which can be correlated with the presence of the libethenite phase detected by XRD, IR and Raman for this sample.

Lishil *et al.* showed using LEIS technique that Ca ions and O ions are more exposed to the first atomic layer of hydroxyapatites, irrespective of the Ca/P ratio.^[15] Therefore the calcium enrichment in the first top layer well explains the formation of $\text{Ca}_2\text{CO}_3\text{H}^+$ ions at the surface of the hydroxyapatites (Figure 5a). The normalized intensity of $\text{Ca}_2\text{CO}_3\text{H}^+$ ions is much bigger for Cu20Hap. Additionally, a semi-quantitative study based on ToF-SIMS showed that the Ca*/P* ratio is 27.4 for Hap support (Figure 5b) and it remains constant after copper addition up to 10 wt% in Cu. However, for the highest copper content (20 wt%), this ratio increases to reach 123.3. This result could be directly linked to the libethenite phase formation. Some phosphates are no more used for hydroxyapatite formation, thus calcium species are able to react with CO_2 to form calcium carbonates (Figure 5a).

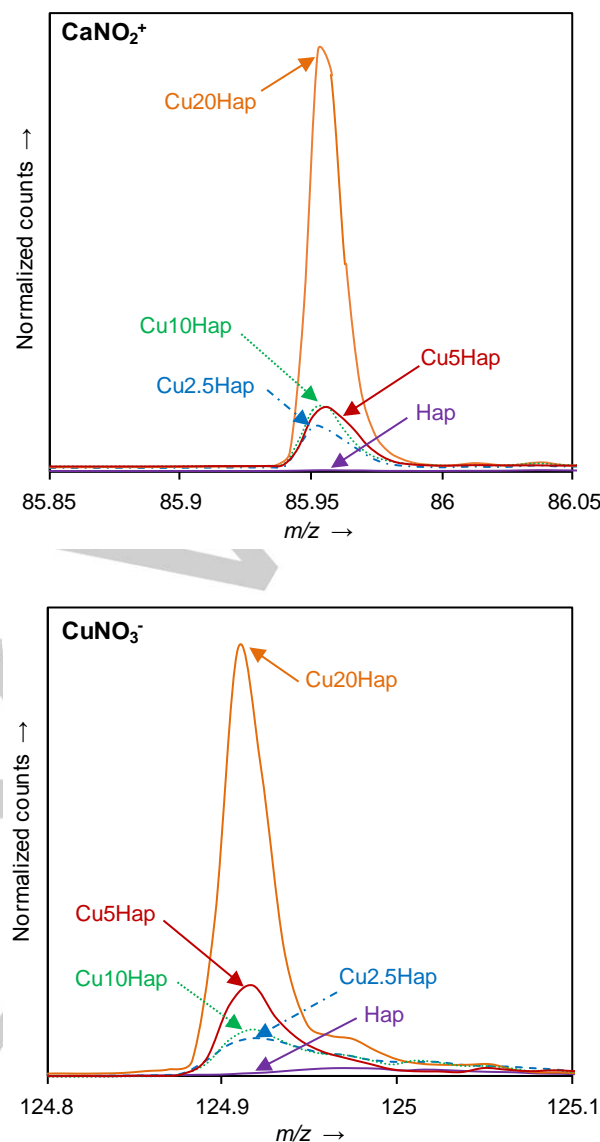


Figure 4. Normalized counts for CaNO_2^+ and CuNO_3^- peaks for CuxHap

FULL PAPER

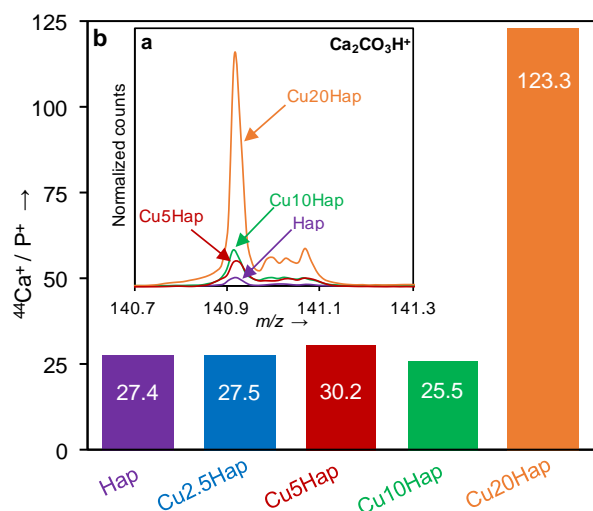


Figure 5. (a) Normalized counts for $\text{Ca}_2\text{CO}_3\text{H}^+$ peak for Hap and Cu5Hap, Cu10Hap and Cu20Hap and (b) Ca^+/P^+ ratio for Hap and CuxHap samples

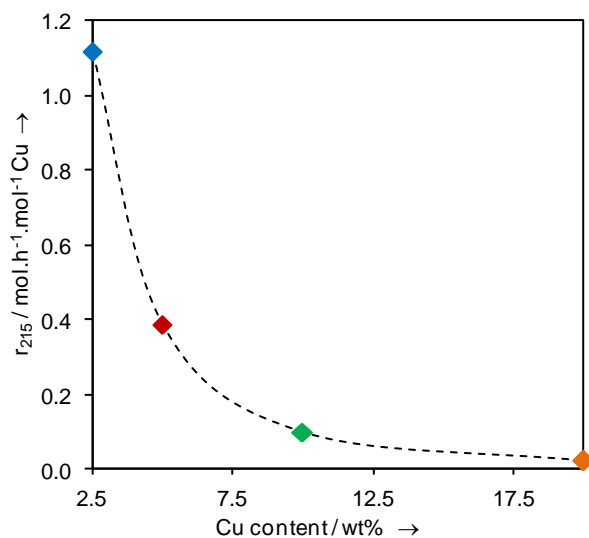


Figure 6. Rate of toluene conversion in function of copper content in CuxHap. Feed composition: 800 ppmv toluene in air, temperature: 215 °C

2. Catalytic performances

2.1. Catalytic oxidation of toluene

The evolution of the toluene conversion into CO_2 over Hap and CuxHap catalysts in function of temperature is illustrated in **Figure S4**. T_{10} , T_{50} and T_{90} , the temperatures at which 10 %, 50 % and 90 % of toluene are converted into CO_2 respectively, have been extracted from these light-off curves and are listed in **Table 3**. It is worth to note traces of benzene and benzaldehyde products in the temperature range [130–220 °C] when toluene is not fully converted.

Cu addition remarkably enhances the toluene conversion of the Hap support. 90 % of toluene conversion is achieved for Cu based catalysts at temperature below 277 °C while for pure Hap the required temperature is higher than 400 °C. Toluene conversion into CO_2 based on T_{50} (°C) decreases as follows: Cu2.5Hap (215) > Cu5Hap (220) > Cu10Hap (232) > Cu20Hap (248) >> Hap (390). Thus the improvement in toluene conversion observed over CuxHap seems to be related to the decrease in the copper content in the sample. Then the catalytic activity was compared by expressing the rate of toluene conversion per mole of copper and evaluated at 215 °C (r_{215}) (**Figure 6**). Similar order of decreasing activity ($\text{mol.h}^{-1}.\text{mol}^{-1}\text{Cu}$) was obtained: Cu2.5Hap (1.116) > Cu5Hap (0.385) > Cu10Hap (0.096) >> Cu20Hap (0.019). It is clear that the catalyst with the lower copper loading has by far the highest rate: r decreased by ten and sixty times when the reaction was performed on Cu10Hap and Cu20Hap respectively instead of Cu2.5Hap.

The apparent energy activation E_A values for toluene oxidation over CuxHap catalysts have been calculated from the Arrhenius plots (**Figure S5**). E_A value depends on the copper content in the sample (**Table 3**). The lower the E_A value is, the easier the toluene can be oxidized. The values of E_A over CuxHap were close to those ($\sim 100 \text{ kJ.mol}^{-1}$) over $\text{CuO}/\text{Al}_2\text{O}_3$.^[38] The lowest E_A value for Cu2.5Hap well explained the highest activity of this catalyst in the toluene oxidation.

Table 4 lists the catalytic properties (T_{50}) of various Cu based materials obtained in toluene (various concentrations) total oxidation. Clearly this comprehensive overview highlights the remarkable catalytic activity of Cu2.5Hap materials. In particular Wang^[10] and Kim^[39] have both investigated the catalytic oxidation of toluene over Cu-based $\gamma\text{-Al}_2\text{O}_3$ catalysts, Cu loading varying from 1 to 15 wt%. They reported 5 wt% $\text{Cu}/\gamma\text{-Al}_2\text{O}_3$ as the most active catalyst owing to the well-dispersed copper (+II) species at the alumina surface. Above 5 wt% Cu content in the sample, large CuO crystals formation led to the catalytic activity decrease. Therefore the better activity achieved over Cu2.5Hap for toluene oxidation can be related to the presence of well dispersed Cu species on the hydroxyapatite. Increasing the copper content in the sample led to the formation of CuO with higher crystallite size (**Table 1**) which are less active in toluene oxidation. The huge promotion of the activity per mol of copper (**Figure 6**) puts forward that the copper dispersion is not the sole parameter influencing the catalytic activity. Besides comparing the catalytic performance of Cu2.5Hap to that of $\text{Cu5\%/Al}_2\text{O}_3$,^[39] the T_{50} is lowered by 60 °C suggesting that the Hap support could contribute to activity increase. Soylu *et al.*^[40] and Carabineiro *et al.*^[13] showed that the acidity of the catalyst plays a dominant role in toluene oxidation reaction. The toluene adsorption takes place with methyl and phenyl groups interaction with the catalyst surface, followed by H and C subtraction.^[41–43] In particular Carabineiro *et al.*^[13] proposed

FULL PAPER

that toluene must be not too strongly adsorbed (weak acid sites) in order to favor afterward the oxygen attack from the surface/lattice of the catalyst. It is well known that hydroxyapatites are not inert supports and can develop both acid and basic sites.^[15] In Hap, Ca^{2+} and HPO_4^{2-} ions can act as Lewis and Brønsted acid sites, respectively. Therefore the possible presence of such ions at the surface of low copper content material could also contribute to the increased catalytic performance of Cu2.5Hap. In this regard further characterization of Cu_xHap acid-base properties are required in order to assess the importance of such properties of Hap in the toluene oxidation.

Table 4. Toluene content in air, Volume Hourly Space Velocity VHSV or Gas Hourly Space Velocity GHSV and temperature at 50 % toluene conversion into CO_2 , T_{50} , on our best catalyst and different copper systems from the literature

Catalyst	Toluene / ppm	VHSV / $\text{m}^3 \cdot \text{kg}^{-1} \cdot \text{h}^{-1}$ (GHSV) / h^{-1}	T_{50} / °C	Reference
Cu2.5Hap	800	30 (15000)	215	present work
5% Cu/ γ - Al_2O_3	4000	3.6	~ 275	[10]
8% CuO/ $\text{Ce}_{0.8}\text{Zr}_{0.2}\text{O}_2$	4400	(33000)	207 ^[a]	[12]
15% Cu/ γ - Al_2O_3	1000	200	305 ^[a]	[38]
5% Cu/ γ - Al_2O_3	900	6	275 ^[a]	[39]
9.5% CuO/HCLT	1000	(15000)	330	[40]
9% Cu/SBA-16	880	(1.2)	~ 337 ^[a]	[44]
10% CuO/ SiO_2	880	(1.2)	~ 317	[45]
10% CuO/SBA-15	880	(1.2)	~ 325	[45]
5% Cu/ ZrO_2	1000	60	~ 245 ^[a]	[46]

[a] Temperature at 50 % toluene conversion

2.2. Stability tests

The stability of the Cu2.5Hap and Cu10Hap catalysts was evaluated by a long-run testing at 215 °C for 45 h (Figure 7). Cu2.5Hap and Cu10Hap exhibit an increase of toluene conversion from 45 % to 67 % and 18 % to 32 % respectively during the first six hours under the stream, and remained stable till the end of the stability test. This result has demonstrated a remarkable behavior of these materials since they do not deactivate under our experimental conditions but instead activate in the first hours to remain stable thereafter. The XRD analyses (not shown) of the samples after stability test did not show any structural modification. An increase in SSA value is observed for used Cu10Hap (Table 1), while it remains the same for used Cu2.5Hap. Interestingly, the ToF-SIMS analyses allow to conclude that nitrates species are consumed during the toluene catalytic oxidation at 215 °C (Figure S6). Redox mechanism is often proposed for the VOC oxidation over transition metal oxides.^[47] Following the reduction of Cu^{2+} to Cu^0 by toluene, the nitrates could be reduced into gaseous N_2 on metallic copper. Besides the amounts of experimental H_2 consumed during H_2 -TPR experiments for the Cu-Hap samples were much higher than the ones obtained theoretically for the reduction of Cu^{2+} species into Cu^0 . As residual NO_3^- coming from the Cu precursor and CO_3^{2-} incorporated in Hap are potential reducible species, their

reduction may contribute to the H_2 consumption and makes the interpretation of the reducibility of copper by H_2 -TPR impossible. Therefore the activation of the catalysts during the first six hours and the increase of SSA value of Cu10Hap in comparison with SSA value of fresh Cu10Hap which contains higher nitrates content could be explained by the reduction of these species.

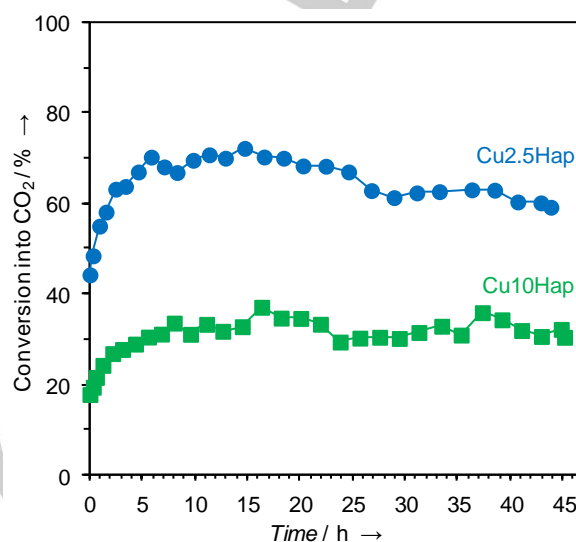


Figure 7. Time-on-stream plot of toluene conversion into CO_2 over Cu2.5Hap and Cu10Hap catalysts. Feed composition: 800 ppm toluene in air, temperature: 215 °C

Conclusions

In this study we have shown that hydroxyapatite-supported copper materials prepared by the wet impregnation method have a great potential as noble metal-free based catalysts for the toluene removal. Copper exchange with hydroxyapatite led to the libethenite phase when high copper content (20 wt%) is deposited on the support. Such copper based phase ($\text{Cu}_2(\text{PO}_4)\text{OH}$) is not very active in the toluene oxidation. However the lowest copper content (2.5 wt%), impregnated over hydroxyapatite support led to the best catalyst for toluene total oxidation owing to well dispersed CuO species and possibly to the participation of the hydroxyapatite in the toluene activation. Despite of the presence of residual NO_3^- species after calcination step at 400 °C, the catalytic performances of Cu/Hap are very stable for 45 h time-on-stream, the nitrates being eliminated by reduction through a redox mechanism implying metallic copper.

Experimental Section

1. Synthesis of the Hap support and supported Cu catalysts

The hydroxyapatite support was prepared as follows ^[15] : 0.0835 mole of $\text{Ca}(\text{NO}_3)_2 \cdot 4\text{H}_2\text{O}$ (Sigma-Aldrich, purity $\geq 99.9\%$)

FULL PAPER

placed in 150 mL of distilled water was added dropwise, under stirring and at 80 °C to 500 mL of an aqueous solution containing 0.05 mole of $(\text{NH}_4)_2\text{H}_2\text{PO}_4$ (Sigma-Aldrich, purity $\geq 98.0\%$). The pH of the solution was kept at 10 during synthesis by adding a 25% $\text{NH}_3\cdot\text{H}_2\text{O}$ solution. The obtained precipitate was filtered, washed with hot water, and dried overnight at 80 °C. The solid was finally calcined at 400 °C for 4 h under air flow. The Ca/P atomic ratio was found to be 1.79.

Several copper-loaded hydroxyapatites were prepared by the conventional impregnation method carried out in a rotary evaporator with 50 mL of copper nitrate $\text{Cu}(\text{NO}_3)_2\cdot 3\text{H}_2\text{O}$ (Sigma Aldrich, purity: 99.1 %) solution containing the appropriate amount of Cu and 2 g of Hap. The resulting mixture was heated at 60 °C. The residue was then dried overnight at 80 °C and calcined 4 h at 400 °C under air flow. The solids are noted Cu_xHap , where x represents the copper weight percentage of Cu ($x= 2.5, 5, 10$ and 20).

2. Characterization of the materials

2.1. Elemental analyses

Quantification of Cu, Ca and P content was done by inductively coupled plasma-optical emission spectroscopy (ICP-OES). Analyses were carried out on an Agilent Technologies 700 Series spectrometer (REALCAT platform - Lille University). For analysis five milligrams of solid were dissolved in 50 mL *aqua regia* solution.

2.2. X-ray diffraction analyses

Powder X-ray diffraction data were recorded on a Bruker AXS D8 Advance diffractometer functioning at room temperature in a Bragg–Brentano geometry. This instrument is equipped with a LynxEye Super Speed detector. Data were collected using the $\text{Cu K}\alpha$ line in a 2θ range from 10 to 65° with a step size of 0.02° and 5 s counting time per step. LaB_6 standard sample was used to determine the instrument resolution. The mean crystallite size of the copper oxides was evaluated by Rietveld refinement. For peak profiles description the Thompson–Cox–Hastings pseudo-Voigt function was selected. Here, an anisotropic size broadening model based on linear combination of spherical harmonics was used to simulate the size broadening, and 6 additional parameters were refined. From this refinement, the individual size of Hap crystallite was derived for each crystallographic plane. From the refinement, the integral breadth of each peak was deduced and the corresponding crystallite size was calculated using the Scherrer formula ($D=\lambda/\beta\cos\theta$ where λ is the wave length, β the integral breadth and θ the peak position).

2.3. N_2 physisorption analyses

Textural properties (specific surface area, pore volume and diameter) of materials were investigated by the physisorption technique which have been carried out by the Micromeritics Tristar II analyser. Before nitrogen adsorption, the solids were outgassed under vacuum at 200 °C for 4 h.

2.4. Infrared spectroscopy experiments

Fourier-transform transmission infrared (FT-IR) spectra were recorded on a Nicolet 460 spectrometer at room temperature. A KBr pellet containing the compound was prepared by intimately mixing about 1 mg of powdered sample with 100 mg of dry powdered KBr. The spectral range covered was 500 to 4000 cm^{-1} with 2 cm^{-1} spectral resolution.

2.5. Raman spectroscopy

The Raman spectra were recorded in air at room temperature using a Raman microprobe (Labram HR). This system incorporated a Peltier-cooled detector and an Ar^+ -ion laser (488 nm) with $\pm 1.5 \text{ cm}^{-1}$ spectral resolution, 0.4 mW laser power and 120 seconds acquisition time for each scan. The presented spectra corresponded to the average of 3 scans. The Raman spectrometer was standardized by means of Si line at 520.6 cm^{-1} .

2.6. X-ray photoelectron spectroscopy

XPS analyses were done on an AXIS Ultra DLD Kratos spectrometer. This instrument operated with a monochromatised source ($\text{Al K}\alpha = 1486.7 \text{ eV}$) and a charge compensation gun. C 1s binding energy at 285 eV was used as reference for determination of different core level binding energies. A mixed Gaussian/Lorentzian peak fit procedure was used to simulate the experimental photo-peaks using CasaXPS processing software. For quantitative analysis a nonlinear Shirley background subtraction was applied. XPS quantification included singlet peaks in the form of C 1s, O 1s and N 1s as well as doublet pairs in the form of Ca 2p, Cu 2p and P 2p. The $\text{Cu}/(\text{Ca}+\text{P})$ surface atomic ratio is calculated in order to access to an indirect copper oxide dispersion. An XPS $\text{Cu}/(\text{Ca}+\text{P})$ close to the bulk ratio means that all Cu atoms are visible by XPS, and consequently that size of the copper oxide particles remains below 10 nm (analysis depth of XPS close to this value). If XPS $\text{Cu}/(\text{Ca}+\text{P})$ ratio falls significantly below the bulk ratio, copper oxide forms in large particles ($\gg 10 \text{ nm}$).

2.7. Time of flight - secondary ion mass spectrometry

ToF-SIMS analyses were achieved on a TOF.SIMS 5 spectrometer (ION-TOF GmbH Germany) implemented with a liquid bismuth ion source. The compacted samples were bombarded with a pulsed 25 keV Bi_3^+ primary ion beam rastered over an area of $500 \times 500 \mu\text{m}^2$. Static conditions were ensured with a data acquisition of 100 s (the total fluence does not amount up to $10^{12} \text{ ions}/\text{cm}^2$). A 20 eV pulsed electron flood gun was employed to compensate the charge effects. In these experiments the mass resolution ($m/\Delta m$) was higher than 4000 at $m/z = 159$ for Ca_2PO_3^+ .

3. Catalytic performances measurement

FULL PAPER

Toluene catalytic oxidation experiments were done at atmospheric pressure in a continuous flow fixed bed reactor located in an electrical furnace. For each catalytic run, 200 mg of fresh catalyst were put in the micro reactor. The reactive gas mixture comprised 800 ppmv of toluene diluted in air (100 mL.min⁻¹) corresponding to a Volume Hourly Space Velocity (VHSV) of 500 mL.g⁻¹.min⁻¹ (30 m³.kg⁻¹.h⁻¹). Before each run, the samples were pretreated 2 h at 390 °C under air flow of 75 mL.min⁻¹. Catalysts performances were evaluated in the 390-30°C temperature range, with a decreasing rate of 0.5 °C.min⁻¹. The concentrations of the gaseous reactants and products were analyzed on line by a 7860A Agilent Gas Chromatography equipped with two detectors (TCD and FID) connected respectively to two columns (Restek Shin Carbon ST/Silco HP NOC 80/100 micro packed and capillary column Cp-Wax52CB25 m, Ø = 0.25 mm).

Toluene conversion into CO₂ was evaluated by:

$$C_{\text{CO}_2}(\%) = \frac{[\text{CO}_2]_i \times 100}{7 \times [\text{toluene}]_i}$$

where [CO₂]_i was the CO₂ outlet concentration and [toluene]_i the toluene inlet concentration.

The rate of toluene conversion expressed in mole of reacted toluene per mole of copper and per hour was calculated owing to the following formula:

$$r = \frac{F \times C_{\text{CO}_2}}{n_{\text{Cu}}}$$

where F is the flow rate of toluene in mole per hour and n_{Cu} the molar amount of copper.

The apparent energy of activation (E_A) of the catalytic reaction for the different catalysts was determined for toluene conversion below 20 %. For a supposed first-order reaction with respect to toluene, the values of apparent rate constant k_{APP} were calculated by k_{APP} = -ln(1-C_{CO2})/τ where τ is the residence time based on the catalyst volume. E_A values were obtained by plotting ln(k_{APP}) vs 1/T.

For long-term testing, the catalysts were first pretreated with air (75 mL.min⁻¹) at 300 °C (10 °C.min⁻¹). After this pretreatment, the samples were cooled to 215°C (10 °C.min⁻¹) and the long-term stability test was conducted at this temperature for 45 hours in toluene (800 ppmv)/air mixture (100 mL.min⁻¹). The catalysts after such long-term testing were labelled CuxHapU.

Acknowledgements

The authors thank the Chevreul Institute (FR 2638) for its help in the development of this work. Chevreul Institute is supported by the « Ministère de l'Enseignement Supérieur et de la Recherche », the « Région Hauts de France » and the « Fonds Européen de Développement des Régions ». This research has been partially supported by a French-Lebanese research project (PHC CEDRE n° 32933QE), a grant from the Lebanese CNRS 2016-2017 project N° 01-08-15 and ARCUS E2D2 project. Mrs D. Chlala and M. Labaki acknowledge the award of a doctoral and research

fellowships by the Agence Universitaire de la Francophonie (AUF) – Région du Moyen-Orient. The authors are grateful in particular to Prof. Rose-Noëlle Vannier for Rietveld refinements, Martine Trentesaux and Laurence Burylo for XPS and XRD measurements, respectively.

Keywords: Volatile Organic Compound • Catalytic Oxidation • Copper • Toluene • Hydroxyapatite

- [1] J.-F. Lamonier, *Catalysts*, **2016**, *6*(1), 7.
- [2] J. Quiroz, S. Royer, J.-P. Bellat, J.-M. Giraudon, J.-F. Lamonier, *ChemSusChem*, **2013**, *6*, 578-592.
- [3] S. Ojala, S. Pitkäaho, T. Laitinen, N.N. Koivikko, R. Brahmī, J. Gaalová, L. Matejova, A. Kucherov, S. Päivärinta, C. Hirschmann, T. Nevanperä, M. Riihimäki, M. Pirlä, R.L. Keiski, *Top. Catal.* **2011**, *54*, 1224-1256.
- [4] J.K. Edwards, B. Solsona, P. Landon, A.F. Carly, A. Herzing, C. Kiely, G.J. Hutching, *J. Catal.* **2005**, *236*, 69-79.
- [5] M. Hosseini, S. Siffert, H.L. Tidahy, R. Cousin, J.-F. Lamonier, A. Aboukais, A. Vantomme, B.-L. Su, *Catal. Today*, **2007**, *122*, 391-396.
- [6] R. Averlant, S. Royer, J.-M. Giraudon, J.-P. Bellat, I. Bezverkhyy, G. Weber, J.-F. Lamonier, *ChemCatChem*, **2014**, *6*, 152-161.
- [7] J. Quiroz, J.-M. Giraudon, A. Gervasini, C. Dujardin, C. Lancelot, M. Trentesaux, J.-F. Lamonier, *ACS Catal.* **2015**, *5*, 2260-2269.
- [8] M. Zimowska, A. Michalik-Zym, R. Janik, T. Machej, J. Gurgul, R. P. Socha, J. Podobiński, E. M. Serwicka, *Catal. Today*, **2007**, *119*, 321-326.
- [9] D. Romero, D. Chlala, M. Labaki, S. Royer, J.-P. Bellat, I. Bezverkhyy, J.-M. Giraudon, J.-F. Lamonier, *Catalysts*, **2015**, *5*, 1479-1497.
- [10] C.-H. Wang, *Chemosphere*, **2004**, *55*, 11-17.
- [11] S. M. Saqer, D. I. Kondarides, X. E. Verykios, *Top. Catal.* **2009**, *52*, 517-527.
- [12] Q.-F. Deng, T.-Z. Ren, B. Agula, Y. Liu, Z.-Y. Yuan, *J. Ind. Eng. Chem.* **2014**, *20*, 3303-3312.
- [13] S. A. C. Carabineiro, X. Chen, M. Konsolakis, A. C. Psarras, P. B. Tavares, J. J. M. Órfão, M. F. R. Pereira, J. L. Figueiredo, *Catal. Today*, **2015**, *244*, 161-171.
- [14] S. Koutsopoulos, *J. Biomed. Mater. Res.* **2002**, *62*, 600-612.
- [15] L. Silvester, J.-F. Lamonier, R.-N. Vannier, C. Lamonier, M. Capron, A.-S. Mamede, F. Pourpoint, A. Gervasini, F. Dumeignil, *J. Mater. Chem. A*, **2014**, *2*(29), 11073-11524.
- [16] S. D. Sebtī, R. Tahir, R. Nazih, S. D. Boulaajaj, *Appl. Catal. A.*, **2001**, *218*, 25-30.
- [17] L. Silvester, J.-F. Lamonier, J. Faye, M. Capron, R.-N. Vannier, C. Lamonier, J.-L. Dubois, J.-L. Couturier, C. Calais, F. Dumeignil, *Catal. Sci. Technol.* **2015**, *5*, 2994-3006.
- [18] B. Chen, J. Li, W. Dai, L. Wang, S. Gao, *Green Chem.* **2014**, *16*, 3328-3334.
- [19] Z. Qu, Y. Sun, D. Chen, Y. Wang, *J. Mol. Catal. A Chem.* **2014**, *393*, 182-190.
- [20] D. Chlala, M. Labaki, J.-M. Giraudon, O. Gardoll, A. D.-Nowicki, A. Roucoux, J.-F. Lamonier, *C. R. Chimie*, **2016**, *19*, 525-537.
- [21] D. Chlala, J.-M. Giraudon, N. Nuns, C. Lancelot, R.-N. Vannier, M. Labaki, J.-F. Lamonier, *Appl. Catal. B*, **2016**, *184*, 87-95.
- [22] B. Aellach, A. Ezzamarty, J. Leglise, C. Lamonier, J.-F. Lamonier, *Catal. Lett.* **2010**, *135*, 197-206.
- [23] G. Bonel, *Ann. Chim.* **1972**, *7*, 65-88.
- [24] J. C. Elliott, *J. Appl. Cryst.* **1980**, *13*, 618-621.
- [25] S. Kannan, I. A. F. Lemos, J. H. G. Rocha, J. M. F. Ferreira, *J. Solid State Chem.* **2005**, *178*, 3190-3196.
- [26] M. E. Fleet, X. Liu, *Biomaterials*, **2007**, *28*, 916-926.
- [27] N. Elazari, A. Ezzamarty, J. Leglise, L.C. de Ménorval, C. Moreau, *Appl. Catal. A*, **2004**, *267*, 235-240.
- [28] W. Martens, R.L. Frost, *Am. Mineral.* **2003**, *88*, 37-46.

FULL PAPER

- [29] L. Debbichi, M. C. Marco de Lucas, J. F. Pierson, P. Krüger, *J. Phys. Chem. C* **2012**, *116*, 10232-10237.
- [30] R. L. Frost, P. A. Williams, W. Martens, J. T. Klopogge, *J. Raman Spectrosc.* **2002**, *33*, 752-757.
- [31] S. Velu, V. Ramkumar, A. Narayanan, C. S. Swamy, *J. Mater. Sci.* **1997**, *32*, 957-964.
- [32] M. Nishino, S. Yamashita, T. Aoba, M. Okazaki, Y. Moriwaki, *J. Dent. Res.* **1981**, *60*, 751-755.
- [33] R. L. Frost, P. A. Williams, W. Martens, J. T. Klopogge, P. Leverett, *J. Raman Spectrosc.* **2002**, *33*, 260-263.
- [34] G. Penel, G. Leroy, C. Rey, E. Bres, *Calcif. Tissue Int.* **1998**, *63*, 475-481.
- [35] A. Antonakos, E. Liarokapis, T. Leventouri, *Biomaterials*, **2007**, *28*, 3043-3054.
- [36] E. L. Solla, J. P. Borrajo, P. González, J. Serra, S. Chiussi, C. Serra, B. León, M. Pérez-Amor, *Vacuum*, **2008**, *82*, 1383-1385.
- [37] S. Sugiyama, T. Minami, H. Hayashi, M. Tanaka, N. Shigemoto, J. B. Moffat, *Energy Fuels*, **1996**, *10*, 828-830.
- [38] S. M. Saqer, D. I. Kondarides, X. E. Verykios, *Appl. Catal. B.* **2011**, *103*, 275-286.
- [39] S. C. Kim, *J. Hazard. Mater.* **2002**, *91*, 285-299.
- [40] G. S. P. Soylu, Z. Özcelik, I. Boz, *Chem. Eng. J.* **2010**, *162*, 380-387.
- [41] E. Finocchio, G. Busca, V. Lorenzelli, R. J. Willey, *J. Catal.* **1995**, *151*, 204-215.
- [42] B. Irigoyen, A. Juan, S. Larrondo, N. Amadeo, *Surf. Sci.* **2003**, *523*, 252-266.
- [43] X. Tang, Y. Xu, W. Shen, *Chem. Eng. J.* **2008**, *144*, 175-180.
- [44] Á. Szegedi, M. Popova, K. Lázár, S. Klébert, E. Drotár, *Micropor. Mesopor. Mater.* **2013**, *177*, 97-104.
- [45] M. Popova, Á. Szegedi, Z. Cherkezova-Zheleva, A. Dimitrova, I. Mitov, *Appl. Catal. A.* **2010**, *381*, 26-35.
- [46] H. L. Tidahy, S. Siffert, F. Wyrwalski, J.-F. Lamonier, A. Aboukaïs, *Catal. Today*, **2007**, *119*, 317-320.
- [47] U. Menon, V. V. Galvita, G. B. Marin, *J. Catal.* **2011**, *283*, 1-9.

FULL PAPER

Layout 1:

WILEY-VCH

Accepted Manuscript

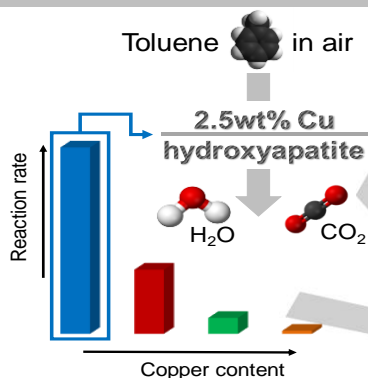
FULL PAPER

Entry for the Table of Contents (Please choose one layout)

Layout 1:

FULL PAPER

Hydroxyapatite supported copper oxides were showed as efficient free noble catalysts for the toluene oxidation. High activity, CO₂ selectivity and stability are achieved over low content Cu materials. Copper in association with hydroxyapatite can be considered as a realistic thinkable material to replace noble metal based solids in VOC oxidation catalytic formulations.



*D. Chlala, J.-M. Giraudon, N. Nuns, M. Labaki, J.-F. Lamonier**

Page No. – Page No.

Cu/Hydroxyapatite: highly active free-noble catalysts for the total oxidation of toluene